Computer Modeling in Engineering & Sciences

Tech Science Press

DOI: 10.32604/cmes.2022.020979

ARTICLE

Numerical Study for Magnetohydrodynamic (MHD) Unsteady Maxwell Nanofluid Flow Impinging on Heated Stretching Sheet

Muhammad Shoaib Arif[1,2,*], Muhammad Jhangir[2], Yasir Nawaz[2], Imran Abbas[2], Kamaleldin Abodayeh[1] and Asad Ejaz[2]

[1]Department of Mathematics and Sciences, College of Humanities and Sciences, Prince Sultan University, Riyadh, 11586, Saudi Arabia

[2]Department of Mathematics, Air University, Islamabad, 44000, Pakistan

*Corresponding Author: Muhammad Shoaib Arif. Email: marif@psu.edu.sa; shoaib.arif@mail.au.edu.pk

Received: 22 December 2021 Accepted: 25 March 2022

ABSTRACT

The numerous applications of Maxwell Nanofluid Stagnation Point Flow, such as those in production industries, the processing of polymers, compression, power generation, lubrication systems, food manufacturing and air conditioning, among other applications, require further research into the effects of various parameters on flow phenomena. In this paper, a study has been carried out for the heat and mass transfer of Maxwell nanofluid flow over the heated stretching sheet. A mathematical model with constitutive expressions is constructed in partial differential equations (PDEs) through obligatory basic conservation laws. A series of transformations are then used to take the system into an ordinary differential equation (ODE). The boundary conditions (BCs) are also treated similarly for transforming into first-order ordinary differential equations (ODEs). Then these ODEs are computed by using the Shooting Method. The effect of factors on the skin friction coefficient, the local Nusselt number, and the local Sherwood number are explored, and the results are displayed graphically. The obtained results demonstrate that by increasing the values of the Maxwell and slip velocity parameters, velocity deescalates. For investigators tasked with addressing unresolved difficulties in the realm of enclosures used in industry and engineering, we thought this work would serve as a guide.

KEYWORDS

Maxwell fluid; stagnation point flow; heat and mass transfer; thermal radiations; shooting method

Nomenclature

$u\,(m/s)$	Horizontal Velocity
$\alpha\,(m^2/s)$	Thermal Diffusivity
$v\,(m/s)$	Vertical Velocity
τ	The Ratio of Heat Capacity of Base Fluid to the Nanoparticles Heat Capacity Coefficient
$\rho_f\,(kg/m^3)$	Density of Fluid
$D_T\,(m^2/s)$	Thermophoretic Parameter

$\nu_f \left(m^2/s\right)$	Kinematic Viscosity
$D_B \left(m^2/s\right)$	Brownian Diffusion Coefficients
$\lambda_1 (s)$	Relaxation Time of Maxwell's Fluid
σ^*	Stefan-Boltzmann Constant
$\sigma \ \left(s^3.m^2/kg\right)$	Electrical Conductivity
k^*	Mean Absorption Coefficient
$B_0(kg/(m^2.s^2))$	Strength of Magnetic Field
δ	Unsteady Parameter
β	Maxwell Parameter
ϵ	Stretching Parameter
P_r	Prandtl Number
R	Thermal Radiation Parameter
N_b	Brownian Motion Parameter
N_t	Thermophoresis Parameter
S_c	Schmidt Number
M	Magnetic Parameter
f_w	Suction/Injection Parameter
$C_w (x, t)$	Volume Fraction of Nanoparticles at the Sheet
C_∞	Volume Fraction of Nanoparticles Farther Apart from the Sheet
$T_w (x, t) \ (K)$	Temperature at the Sheet
$T_\infty (K)$	Temperature Farther Apart from the Sheet
$\vec{B}$	Transverse Magnetic Field
$\bar{J} * \vec{B}$	Lorentz Force
$\bar{J} \left(A/m^2\right)$	Electrical Current Density

1 Introduction

It is a fact that our earth is covered with a hundred per cent air and approximately seventy per cent water. Since water and air are fluids, fluids have great significance in our lives. Archimedes was the mathematician who examined the statics and buoyancy of the fluids. Researchers have shown their great interest in non-Newtonian fluids during the last few decades. Non-Newtonian fluids are the most critical fluids because of their enormous applications in biological sciences, food processing industry, geophysics, oil pipelines, chemical industry, rocket engines, air conditioning systems, petroleum industry, wind turbines, etc. The flow behaviour of non-Newtonian fluids is modified under stress. Most numerous fluids used in biomedicine and industry are non-Newtonian. Some familiar examples are blood, ink, honey, shampoos, slurries, printer, and cosmetic products. Using the Navier-Stokes equations and their constitutive relationship, we may better understand the rheological individuality of Newtonian fluids; on the other hand, non-Newtonian fluids have very different flow characteristics than Newtonian fluids. Several researchers have applied 2D translational magnetohydrodynamic (MHD) techniques to the movement of Maxwell's convection and discovered that these phenomena were important factors in 2D fluid flow caused by gravitational waves. To explore the thermal and mass transfer properties in 2D transient Maxwell nanofluid flow induced by stretching cylinder magnetic field are considered in [1].

Nanofluids are used extensively in nanoscience, including building materials, military equipment, nano machining of nanowires and nanorods, etc. In this regard, the following studies can be consulted [2,3]. Hayat et al. tried to figure out the flow of second-grade fluid, non-linear surface stress,

convective heat, and keeping property of various skins with a tool designed to analyze flow convection [4]. The properties of flow in non-linear geometries were investigated with nanofluid properties for small region solutions [5,6]. Ahmed et al. [7] studied the MHD Magneto hydrodynamic fluid flow through a porous medium with this high surface-to-volume colloidal hydromagnetic nanofluid analysis. The effects of non-linear thermal radiation, convective conditions, and heat generation/absorption at the boundary are investigated to determine whether synergies exist. MHD is a term that refers to the study of electrically conducting fluid dynamics. This is accomplished by combining the Navier-Stokes equations for fluid dynamics and Maxwell's equations for electromagnetism. One of the MHD's important innovations was the recognition that magnetic fields can create currents in a fluid conductor, which induce corresponding currents in the fluid, producing magnetic forces on the fluid. In the presence of zero normal streams of nanoparticle speed-slip boundary conditions, the numerical analysis of stagnation-point flow, convectional heat transmission to the tan-gent nanofluid was studied by Vittal et al. [8]. Numerical surveys on unsteady magnetohydrodynamic MHD in permeability over a stretched sheet with reaction boundary and suction/injection boundary have been studied by Shravani et al. [9]. Srinivas et al. [10] investigated the effects of Soret and convective boundary conditions on MHD pulsating flow in a horizontal channel using an analytical solution based on the perturbation technique. Ramesh et al. [11] analyzed to determine the Maxwell fluid stagnation point in the presence of nanoparticles and a permeable stretching sheet.

Magnetohydrodynamic fluid flow and heat transfer problems for a vicious and incompressible dusty fluid conductor over an unstable stretch panel are solved using numerical analysis by Manjunatha et al. [12]. The effect of heat generation and absorption on tangent hyperbolic nanofluid at the stagnation point over a stretching cylinder was studied by Salahuddin et al. [13]. The unpredictability of MHD free convection flow was investigated by Ahmmed et al. [14]. In the presence of radiation, a nanofluid flows through an exponentially accelerated inclined plate embedded in a porous material with variable thermal conductivity. The work presented in [15] investigates the Newtonian heating properties of a viscous nanomaterial in a permeable stretched flow. In [16], Mondal et al. presented a model for the Maxwell nanofluid's unstable flow through a permeable, convective border shrinking plate and heat transfer.

Nanofluids are suspensions of solid particles whose diameters range from 1 to 100 nm. Nanofluids, including base fluids and nanoparticles, are taken as a subclass for heat transfer fluids. In nanofluids, the nanoparticles are generally made up of nano metals, for instance (carbon, graphite) or metals like Al_2O_3, (Al, Cu) oxides, nitrides (AlN, SiN). Nanofluids are adequately viscous, steady enough against wetting, dispersing, and bear spreading characteristics on solid surfaces, even for modest nanoparticle fixation. These are used to increase the thermo-physical characteristic like heat transfer, viscosity, thermal diffusivity, and base fluid conductivity such as ethylene glycol, propylene glycol, water, etc. With a low concentration (1–5) percent, the thermal conductivity of solid nanoparticles is increased by about 40 percent. It has several applications in engineering and biotechnology, like cancer therapy and the cooling process in industries. These become the two-phase system due to solid and liquid. Many articles have been published to study nanofluids' increased heat transfer capabilities [17–23]. Mustafa et al. [24] discussed thermophoretic Brownian motion and the magnetic field's consequences on the mixed convective flow of magneto-nanofluid that is hurdled by an extendable vertical surface. Hayat looked at the impact of chemical reactions in magnetohydrodynamic flow through a non-linear radially stretching surface. The author concluded that the Nusselt number depends on the power-law index and increases the power-law index function.

Atif et al. [25] presented the idea of magnetohydrodynamic micro polar Carreau nanofluid and reported that thermal profile escalates for larger values of the Brownian motion parameter.

Dogonchi et al. [26] considered thermal flux and thermal radiation consequences and MHD nanofluid heating over a stretching sheet Joule Heating. Cattaneo Christov's heat flux model investigates heat transfer characteristics. Finally, Reddy et al. [27] explored a similar solution in the existence of Thermophoresis and Brownian parameters for hydromagnetic movement of a nanofluid over a slandering stretching sheet. Dogonchi et al. [28] recently investigated the effect of radiation on the heat transfer of nanofluid flow using permeable media. He observed an increment in the velocity and reduction in the temperature profile by enhancing the Reynolds number and expansion ratio. It was stated that the heat transfer rate increases directly by escalating the values of mixed convection parameters. The effects of thermal radiation on nanofluid flow have also been discussed by Sheikholeslami et al. [29,30]. The characteristics of heat transfer and fluid flow, taking into account the nanofluids, were studied in detail by several researchers [31–34]. Recent papers have given several investigations in convective transport using nanofluids in external flow and boundary layer flow [35–38].

Many researchers put their valuable investigations on the Maxwell nanofluids' flow and their further types using different sheets [39–43]. Bilal et al. [44] examined the continual heat and mass transfer features generated by an inclined-cylinder diffusion, heat fluids, convective heating effects, and joule heating effects. Lu et al. [45] studied entropic generation with the effect of magnetic dissipation and transpiration in the dissipative flow of nanofluids. The primary objective of [46] is to investigate the Brownian motion and heat-forging effects on micropolar nanofluid flow on a non-linear inclined stretch sheet while accounting for the effects of Soret and Dufour. In the presence of a non-uniform heat source/sink, the Carreau nanoparticle thin film's thermodynamics is being studied by Khan et al. [47]. In this study, in the presence of suction, heat radiation, and a heat source/sink, Jamaludin et al. [48] numerically investigated the stagnant convection mixture-point flow nanofluid over a vertical stretching/shrinking sheet. Bagherzadeh et al. [49] investigated the effect of a magnetic field on the hot injection of dispersed nanoparticles into a microchannel via a micro cross. According to Jalali et al. [50], oil nanofluid jet injection into a rectangular microchannel was studied for heat transfer. Hajatzadeh Pordanjani et al. [51] examined the effect of free convection in the cavity of the thermal field and thermal radiation of the thermal transfer and entropy generation of nanofluid.

The flow of an incompressible viscous fluid across a flat deformable sheet with a velocity proportional to the distance from the stagnation point is studied in [52]. The work in [53] investigated the steady two-dimensional stagnation point flow of an incompressible micropolar fluid over a stretching sheet when the sheet is extended in its own plane. The flow of an incompressible micropolar fluid over a non-linear stretching surface is investigated in two dimensions [54]. For boundary layer flow over nonlinearly extending sheets, an analytical solution has been provided by the shooting approach in [55]. Variable transverse magnetic field, viscous dissipation, thermal radiation, and a nonlinearly flowing free stream were all considered in the flow analysis. The effect of viscous dissipation has also been considered in [56] for Williamson nanofluid under the effects of multiple slips and Joule heating. The resulting system of ordinary differential equations has been tackled with the shooting method based on the Runge-Kutta-Fehlberg method. Local skin friction coefficients, local heat transfer rates, and mass transfer rates are shown in the tables below. According to [57], a shooting strategy based on the 4th-order Runge-Kutta Gill method was used to solve a set of non-linear ordinary differential equations generated by viscous dissipation. Hybrid nanoparticles' influence on velocity and temperature profiles has been given in [58] over a stretching sheet. The non-linear thermal radiation in the energy equation has been considered despite linearized thermal radiations. The differential transform method has been employed to solve the set of ordinary differential equations that arise in the MHD Williamson fluid with chemical reaction [59]. It was observed that Williamson's fluid parameter and magnetic strength produce a thicker boundary layer for velocity. Another analytical research based on the homotopy

analysis method was presented for the two-dimensional steady, incompressible flow of the Oldroyd-8 constant [60]. The homotopy analysis method is based on homotopy that contains a parameter for controlling the convergence of solution series. The method finds the solution of linear and non-linear ordinary and partial differential equations in components form. The study of entropy optimization of MHD coupe stress nanofluid slip flow and heat & mass transfer on entropy generation has been given in [61,62]. Recent research on boundary layer fluid flow problems is available in [63–66].

The study comprises an extension of the previously constructed model for MHD boundary layer flow. The effects of Maxwell fluid and velocity slip are considered with the existing model. The previous study has consisted of an analytical approach, but in this study, a numerical method based on the Runge-Kutta method and Newton Raphson method. The combination of these methods is called the shooting method, which can find missing initial conditions.

The strategy of this paper is as follows:

We examine classical definitions and a history of unstable boundary layer flow 2-D MHD in Section 2. In Section 3, numerical results are presented using different numerical techniques. Results and discussion are presented in Section 4. Section 5 sums up the findings.

2 Governing Equations

The presented model aimed to investigate a 2-D MHD unsteady boundary layer flow considering the Maxwell nanofluid by considering the fluid flow over a porous stretching surface. Moreover, the impacts of thermal emission and magnetic fields are considered. The 2-D Cartesian coordinate system is taken so that x-axis is taken along the flow and y-axis is taken normal to the sheet. To stretch the sheet in a fixed region, along the x-axis two spontaneous forces are applied, opposite in direction but equal in magnitude. At time $t = 0$, the fluid flow is steady. However, for a time $t > 0$, it will become unsteady. An incompressible and laminar flow is bounded in the section specified as $y > 0$. The sheet is stretched towards the x-axis with velocity $U_w(x,t) = \dfrac{ax}{1-\lambda t}$, here the stretching rate is denoted by a where λ is a positive constant with axiom $\lambda t < 1$. $U_e(x,t) = \dfrac{bx}{1-\lambda t}$ is the velocity of the ambient fluid. There will be no slip between nanoparticles and base fluid for thermal equilibrium. But for electrically conducting fluid $\bar{J} * \bar{B}$ (Lorentz force) is acting on the fluid here, the transverse magnetic field is denoted by $\vec{B} = (0, B, 0)$. The simplified Lorentz force is $-\sigma B_0^2 (u - U_e)$, $B = \dfrac{B_0}{\sqrt{1-\lambda t}}$ is the magnetic field perpendicular to the sheet. According to [63], the induced magnetic field is discarded due to the small magnetic Reynolds number. Also, neglect the induced electrical field due to the polarization of charge, and there does not exist external electric field. The geometry of the problem is given in Fig. 1. The constitutive PDEs for continuity, momentum, energy, and concentration are given below:

$$\frac{\partial u}{\partial x} + \frac{\partial v}{\partial y} = 0 \tag{1}$$

$$\frac{\partial u}{\partial t} + u\frac{\partial u}{\partial x} + v\frac{\partial u}{\partial y} = -\lambda_1 \begin{pmatrix} u^2 \dfrac{\partial^2 u}{\partial x^2} + v^2 \dfrac{\partial^2 u}{\partial y^2} \\ +2uvu \dfrac{\partial^2 u}{\partial x \partial y} \end{pmatrix} + \frac{\partial U_e}{\partial t} + U_e \frac{\partial U_e}{\partial x} + v_f \frac{\partial^2 u}{\partial y^2} - \frac{\sigma B_0^2 (u - U_e)}{\rho_f} \tag{2}$$

$$\frac{\partial T}{\partial t} + u\frac{\partial T}{\partial x} + v\frac{\partial T}{\partial y} = \left(\alpha + \frac{16\sigma^* T_\infty^3}{3k^* \rho c_p}\right) \frac{\partial^2 T}{\partial y^2} + \tau \left[D_B \frac{\partial C}{\partial y}\frac{\partial T}{\partial y} + \left(\frac{D_T}{T_\infty}\right)\left(\frac{\partial T}{\partial y}\right)^2 \right] \tag{3}$$

$$\frac{\partial C}{\partial t}+u\frac{\partial C}{\partial x}+v\frac{\partial C}{\partial y}=D_B\frac{\partial^2 C}{\partial y^2}+\frac{D_T}{T_\infty}\frac{\partial^2 T}{\partial y^2} \tag{4}$$

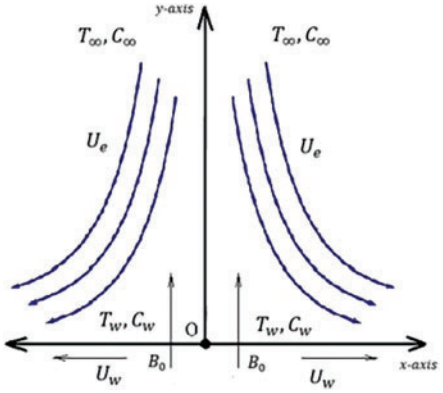

Figure 1: Geometry of the problem

In Eq. (3), a linearized Rosseland radiative flux is considered whose linearized form is given by:

$$q_r=-\frac{4\sigma^*}{3k^*}\frac{\partial T^4}{\partial y}=-\frac{16\sigma^* T_\infty^3}{3k^*}\frac{\partial T}{\partial y}$$

where $\tau=\dfrac{(\rho_c)_f}{(\rho_c)_p}$. At the boundary, the conditions for the model, as mentioned earlier, are as follows:

$$\left.\begin{aligned} u=U_w+\gamma_1\frac{\partial u}{\partial y},\ v=v_w,\ T=T_w,\ C=C_w \quad at \quad y=0\\ u\to U_e,\ T\to T_\infty,\ C\to C_\infty \quad when \quad y\to\infty \end{aligned}\right\} \tag{5}$$

where γ_1 is the slip coefficient while the velocity of suction/injection is denoted by $v_w=\dfrac{v_0}{\sqrt{1-\lambda t}}$. At the boundary, assume the sheet's temperature and nanoparticles volume fraction as [34]:

$$T_w(x,t)=T_\infty+\frac{ax^2}{2v_f(1-\lambda t)^2}T_0,\qquad C_w(x,t)=C_\infty+\frac{ax^2}{2v_f(1-\lambda t)^2}C_0 \tag{6}$$

Here T_0 is a positive reference temperature, and C_0 is positive reference nanoparticles volume fraction such that $T_w>T_0>0$ and $C_w>C_0>0$, these expressions are valid only if $0<(1-\lambda t)$. Now, non-dimensional variables are defined as [34]:

$$\left.\begin{aligned} \eta=\sqrt{\frac{a}{v_f(1-\lambda t)}}y,\quad \psi=\sqrt{\frac{av_f}{(1-\lambda t)}}xf(\eta)\\ T(x,y,t)=T_\infty+\frac{ax^2}{2v_f(1-\lambda t)^2}\theta(\eta),\quad C(x,y,t)=C_\infty+\frac{ax^2}{2v_f(1-\lambda t)^2}\phi(\eta) \end{aligned}\right\} \tag{7}$$

The components of velocity are defined as [34]:

$$u=\frac{ax}{1-\lambda t}f'(\eta),\quad v=-\sqrt{\frac{av_f}{1-\lambda t}}f(\eta)$$

Here differentiation with respect to η is denoted by prime. Now using Eqs. (6) and (7) into dimensional Eqs. (2) to (4), the following non-dimensional system of ODEs can be obtained:

$$f''' + \beta\left(2ff'f'' - f^2f'''\right) + ff'' - f'^2 - \delta\left(f' + \frac{\eta f''}{2}\right) + M^2\left(\epsilon - f'\right) + \delta\epsilon + \epsilon^2 = 0 \tag{8}$$

$$\frac{1}{P_r}\left(1 + R\right)\theta'' + f\theta' - 2f'\theta - \delta\left(2\theta + \frac{\eta\theta'}{2}\right) + N_t\theta'^2 + N_b\theta'\phi' = 0 \tag{9}$$

$$\phi'' + Sc\left(f\phi' - 2f'\phi\right) - Sc\delta\left(\frac{\eta}{2}\phi' + 2\phi\right) + \frac{Nt}{Nb}\theta'' = 0 \tag{10}$$

Eqs. (3)–(4) & (9)–(10) are same given in [34]. The transformed non-dimensional boundary conditions are:

$$\left.\begin{array}{l} f\left(0\right) = f_w,\ f'\left(0\right) = 1 + \gamma f''\left(0\right),\ \theta\left(0\right) = 1,\ \phi\left(0\right) = 1 \\ f' \to \varepsilon,\ \theta \to 0, \quad \phi \to 0, \quad when\ \eta \to \infty \end{array}\right\} \tag{11}$$

where parameters are given below:

$$\delta = \frac{\lambda}{a}, \epsilon = \frac{b}{a}, P_r = \frac{v_f}{\alpha}, \beta = \frac{\lambda_1 a}{1 - \lambda t},\ R = \frac{16T_\infty^3\sigma^*}{3kk^*}, N_b = \frac{\tau D_B\left(C_w - C_\infty\right)}{v_f},$$

$$N_t = \frac{\tau \mathrm{D_B}\left(T_w - T_\infty\right)}{T_\infty v_f}, S_c = \frac{v_f}{D_B}, M = \sqrt{\frac{\sigma}{a\rho_f}}B_0, f_w = \frac{v_0}{\sqrt{av_f}}$$

Dimensional skin friction coefficient (without the effect of Maxwell fluid), local Nusselt and Sherwood numbers are as under:

$$C_f = \frac{\mu}{\rho_f U_w^2}\left(\frac{\partial u}{\partial y}\right)_{y=0} \tag{12}$$

$$N_u = -\frac{x}{k\left(T_w - T_\infty\right)}\left[k\left(\frac{\partial T}{\partial y}\right) + \frac{16\sigma^* T_\infty^3}{3k^*}\left(\frac{\partial T}{\partial y}\right)\right] \tag{13}$$

$$S_h = -\frac{x}{C_w - C_\infty}\frac{\partial C}{\partial y} \tag{14}$$

The non-dimensional forms of Eqs. (12) to (14) can be expressed as:

$$C_{fr} = \sqrt{Re_x C_f} = f''\left(0\right) \tag{15}$$

$$N_{ur} = \frac{N_u}{\sqrt{Re_x}} = -\left(1 + R\right)\theta'\left(0\right) \tag{16}$$

$$S_{hr} = \frac{S_h}{\sqrt{Re_x}} = -\phi'\left(0\right) \tag{17}$$

Here the Reynolds number is:

$$Re_x = x\frac{U_w}{v_f} \tag{18}$$

3 Numerical Treatment

The present section is related to the implementation of the shooting method. A system of higher-order ODEs is converted into first-order ODEs along with the boundary conditions. The shooting method is based on applying the Runge-Kutta method to discretize the set of ordinary differential equations. The Newton Raphson method is employed to find missing initial conditions. Since the Runge-Kutta method is applied to first-order differential equations, the equations are reduced into first-order differential equations.

Following notations are used for converting Eqs. (8)–(10) into first-order ODEs:

$$f = g_1,\ f' = g_2,\ f''' = g_3,\ \theta = g_4,\ \theta' = g_5,\ \phi = g_6,\ \phi' = g_7$$

Now using the above notations, we convert Eqs. (8)–(10) into a system of first-order ODEs along with their given and assumed boundary conditions:

$$g_1' = g_2;\ g_1(0) = f_w$$

$$g_2' = g_3;\ g_2(0) = s_1$$

$$g_3' = \frac{1}{1-\beta g_1^2}\left[\begin{array}{c} -2\beta g_1 g_2 g_3 - g_1 g_3 + g_2^2 + \delta\left(g_2 + \frac{\eta}{2} g_3\right) \\ -M(\varepsilon - g_2) - \delta\varepsilon - \varepsilon^2 \end{array}\right];\ g_3(0) = s_2$$

$$g_4' = g_5;\ g_4(0) = 1$$

$$g_5' = \frac{Pr}{1+R}\left[\begin{array}{c} -g_1 g_5 + 2g_2 g_4 + \frac{\lambda}{a}\left(2g_4 + \frac{\eta}{2} g_5\right) \\ -N_t g_5^2 - N_b g_5 g_7 \end{array}\right];\ g_5(0) = s_3$$

$$g_6' = g_7;\ g_6(0) = 1$$

$$g_7' = -Sc(g_1 g_7 - 2g_2 g_6) + Sc\delta\left(\frac{\eta}{2} g_7 + 2g_6\right) - \frac{N_t}{N_b} g_5';\ g_7(0) = s_4$$

The approximate solution of the above first-order ODEs is obtained by incorporating the RK-4 method and an iterative method. The chosen domain for the problem is $[0, \eta_\infty]$. Here η_∞ is a finite real number such that variation for solution in $\eta > \eta_\infty$ is ignorable. Newton's iterative scheme is used to solve the algebraic equations, which is given as follows:

$$s_{i,n+1} = s_{i,n} - \frac{\left(g_j(\eta_\infty)\right)_{s_i = s_{i,n}} - \varepsilon}{\frac{\partial}{\partial s_i}\left(g_j(\eta_\infty)\right)_{s_i = s_{i,n}}}$$

where $i = 1, 2, 3$ & $j = 3, 5, 7$. If we meet the criterion:

$$\left|\left(g_j(\eta_\infty)\right)_{s_i = s_{i,n}} - \varepsilon\right| > \varepsilon_0$$

Then we will stop the computational processes; otherwise, we continue using the Newton iterative scheme to refine the initial guess. Here ε_0 is a very small positive number.

4 Result and Discussion

We thoroughly discuss approximated results of Skin-friction, Nusselt number, and Sherwood number through graphs. Calculations were carried out to influence different non-dimensional parameters like M, N_b, N_t, S_c and R through the shooting method. Moreover, the impact of these parameters on concentration, temperature, and velocity profiles is also considered via graphs.

Fig. 2 is defined for various values of M against the non-dimensional velocity profile. We observed that the non-dimensional velocity profile escalates with the escalation of magnetic parameter M. Also, the velocity profile was found to be a decline for suction. Fig. 3 is plotted in the existence of injection. To delineate the impact of parameter M on non-dimensional velocity, the velocity profile seems to decline for the rising values of M. It appears to decline for the escalating values of M.

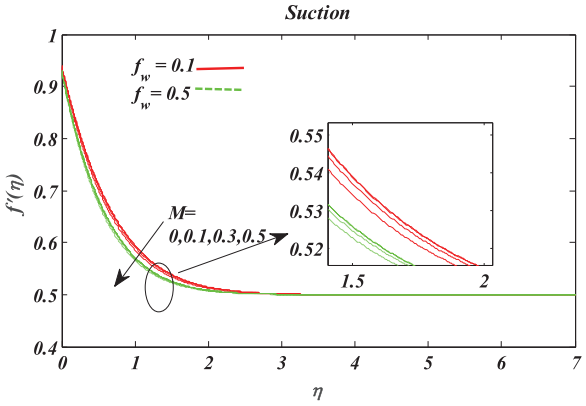

Figure 2: Effect of magnetic parameter M on $f'(\eta)$

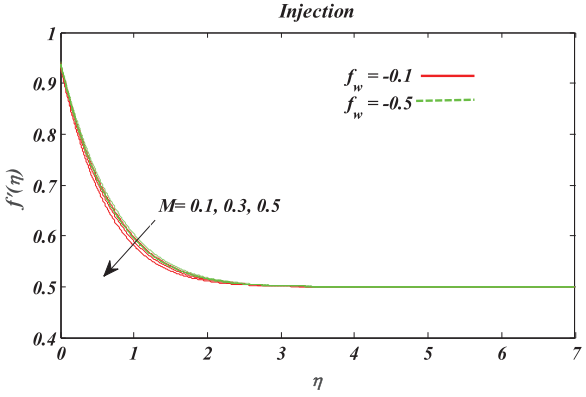

Figure 3: Effect of magnetic parameter M on the velocity profile using $Pr = 1.2,\ \varepsilon = 0.1,\ Nb = Nt = 0.2,\ Sc = 01,\ R = 0.5,\ \delta = 0.1,\ \beta = 0.2$

The effect of δ for various values on non-dimensional velocity profiles is displayed in Figs. 4 to 5. With the rise in unsteady parameter δ, the non-dimensional velocity deescalates and escalates, respectively, for suction and injection. Figs. 6 and 7 are plotted for the dimensionless velocity against the different values of Maxwell parameter β for suction/injection. The figures reflect that the dimensionless velocity profile deescalates and escalates for suction and injection with the Maxwell parameter β.

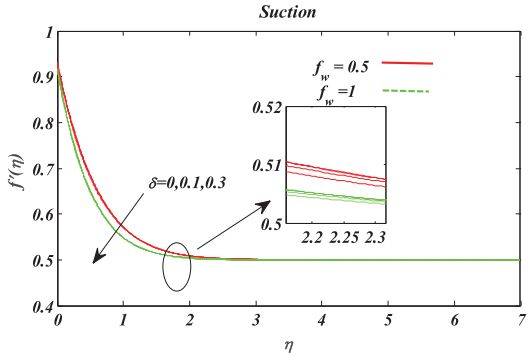

Figure 4: Effect of unsteady parameter δ on the velocity profile using $Pr = 1.2,\ \varepsilon = 0.1,\ Nb = Nt = 0.2,\ Sc = 01,\ R = M = 0.5$

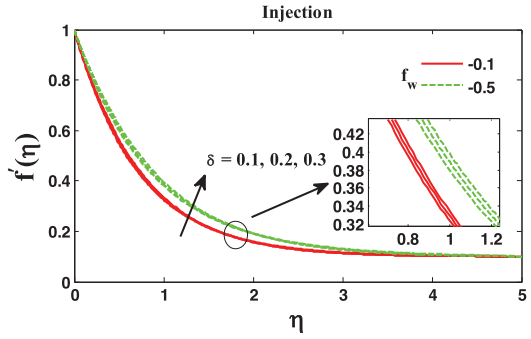

Figure 5: Effect of unsteady parameter δ on the velocity profile using $Pr = 1.2,\ \epsilon = 0.1,\ Nb = Nt = 0.2,\ Sc = 01,\ R = M = 0.5$

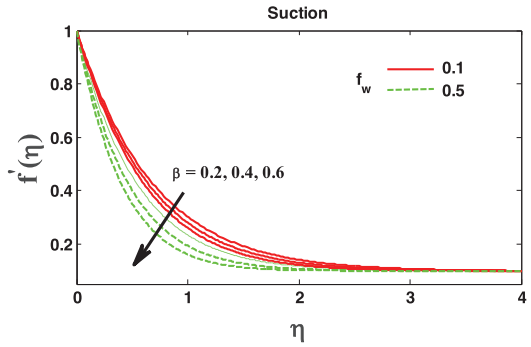

Figure 6: Effect of maxwell parameter β on the velocity profile using $Pr = 1.2,\ \epsilon = 0.1,\ Nb = Nt = 0.2,\ Sc = 01,\ R = M = 0.5,\ \delta = 0.1$

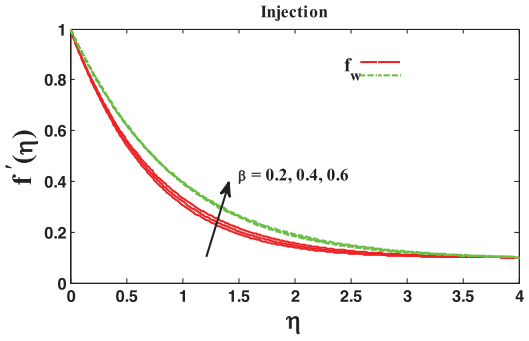

Figure 7: Effect of maxwell parameter β on the velocity profile using $Pr = 1.2,\ \epsilon = 0.1,\ Nb = Nt = 0.2,\ Sc = 01,\ R = M = 0.5,\ \delta = 0.1$

Figs. 8 and 9 are framed to delineate the effect of parameters f_W and M on non-dimensional temperature distribution $\theta\,(\eta)$. Fig. 8 exhibits that the temperature distribution escalates with the escalation in various values in the magnetic parameter and the suction parameter f_W. Similar behaviour has been observed for injection in Fig. 9. The dimensionless temperature profile is enhanced due to the transverse magnetic field M because the flow field is reduced due to magnetic parameter M in both cases.

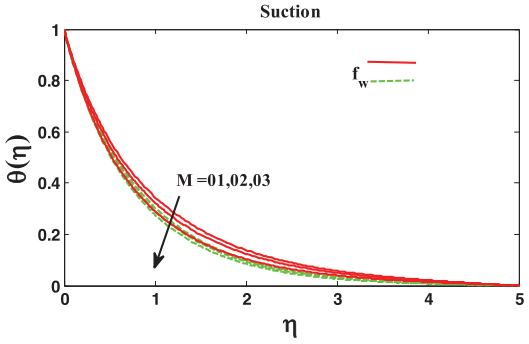

Figure 8: Effect of magnetic parameter M on the velocity profile using $Pr = 1.2,\ \epsilon = 0.1,\ Nb = Nt = 0.2,\ Sc = 01,\ R = 0.5,\ \delta = 0.1,\ \beta = 0.2$

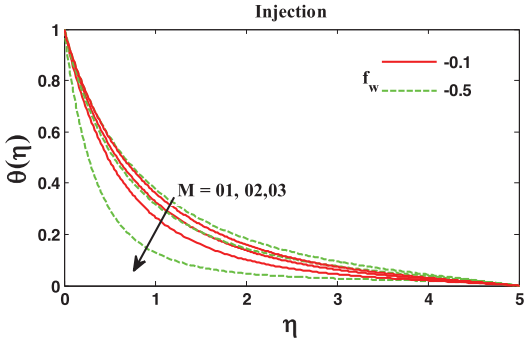

Figure 9: Effect of magnetic parameter M on the temperature profile using $Pr = 1.2,\ \epsilon = 0.1,\ Nb = Nt = 0.2,\ Sc = 01,\ R = 0.5,\ \delta = 0.1,\ \beta = 0.2$

Fig. 10 demonstrates the impact of the parameters R and δ on the non-dimensional temperature profile. It is clear from Fig. 10 that a large estimation of the parameter δ deescalates the non-dimensional temperature for the inner thermal boundary layer. Resultantly, the thermal boundary layer thickness is decreased. Moreover, an increment in R escalates the heat flux from the sheet, which upraises the temperature, and consequently, the non-dimensional temperature profile is enhanced with the increment in R. Whereas Fig. 10 describes the impact of parameters N_t and N_b on the non-dimensional temperature. As a consequence of the particles' random motion, the particles' collision rate increases. Resultantly, the kinetic energy of the particles enhances. This is transformed into heat energy. Hence with an enhancement in the Brownian motion parameter N_b, the non-dimensional temperature escalates.

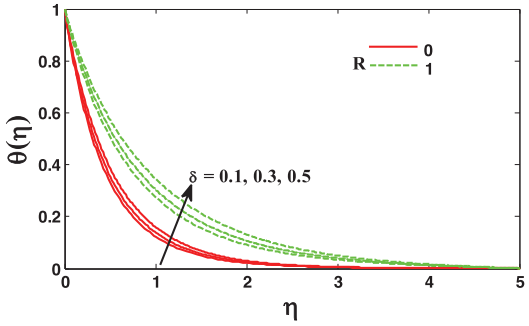

Figure 10: Effect of unsteady parameter δ on the temperature profile using $Pr = 1.2,\ \epsilon = 0.1,\ Nb = Nt = 0.2,\ Sc = 01,\ M = 0.5,\ \mathrm{f}_w = 0.5,\ \beta = 0.2$

Similarly, the temperature profile $\theta\ (\eta\ )$ seems to incline with N_t Inclination because the gradient of temperature generates a force. This is because heated fluid shifted away from the surface, which increases the thermophoresis parameter N_t. Consequently, the boundary layer temperature seems to be enhanced, as delineated in Fig. 11.

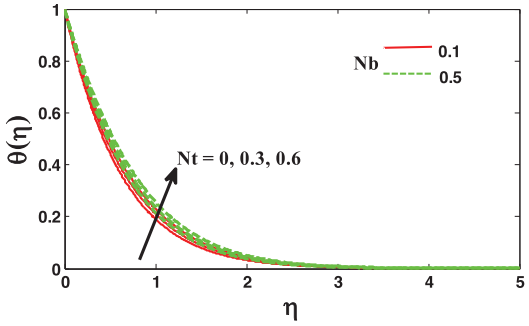

Figure 11: Effect of thermophoresis parameter N_t on temperature profile using $Pr = 1.2,\ \epsilon = 0.1,\ \delta = R = 0.1,\ Sc = 01,\ M = 0.5,\ \mathrm{f}_w = 0.2,\ \beta = 0.2$

Fig. 12 delineates the concentration profile with the variation of thermophoretic parameter N_t and Brownian motion parameter N_b. The concentration profile grows by enhancing thermophoretic and Brownian motion parameters N_t & N_b. Similarly, Fig. 13 reveals the impact of the thermophoretic parameter and Brownian motion parameter N_t and N_b on concentration profile. It seems to be a concentration profile upraises by enhancing the values of both parameters. Because increasing the

Brownian motion parameter leads to the displacement of nanoparticles from the plate to its surroundings, the concentration profile is elevated. Fig. 14 clarifies the impact of velocity slip parameter γ on the velocity profile. It seems to be velocity deescalates by decaying the values of the slip velocity parameter γ. Since upraising, the values of the slip parameter upraises the coefficient of shear stress at the plate, which results from resistance in the fluid motion near the plate. So, the velocity of the adjacent layers of the fluid decays. Fig. 15 reveals the impact of the Schmidt number S_c on concentration profile. The concentration profile deescalates by enhancing Schmidt's number S_c because growth in the values of the Schmidt number S_c either grows the kinematic viscosity of different base fluids or decays the mass diffusivity. For the first case of growing viscosity, the fluid's velocity deescalates, responsible for deescalating the concentration profile for the second case of decaying mass diffusivity. Smaller values of mass diffusivity deescalate the concentration profile due to Fick's law. Fig. 16 exposes the impact of magnetic parameter M and unsteady parameter δ on local Nusselt numbers. The local Nusselt number decays by raising the values of magnetic parameter M because the rising strength of the magnetic field resists the flow's velocity. This results in decay in convective heat transfer, so the local Nusselt number decreases. Also, the local Nusselt number grows by enhancing the values of the unsteady parameter. Fig. 17 delineates the impact of the Schmidt number S_c and Brownian motion parameter N_b on local Sherwood number. The local Sherwood number upraises by enhancing the Schmidt number and Brownian motion parameter values. The growth in Schmidt number leads to decay in mass diffusion rate, so the local Sherwood number is enhanced. Also, an increase in the Brownian motion parameter leads to growth in random movements of particles, and therefore convective mass transfer escalates, and thus local Sherwood number increases. Fig. 18 demonstrates the impact of thermal radiation parameter R and thermophoretic parameter N_t on local Nusselt number. The local Nusselt number rises by enhancing the values of the radiation parameter. The reason behind the growth of local Nusselt number is the escalation of conductive heat transfer due to incoming radiations when radiation parameter increases. The local Nusselt number decays by increasing the values of the thermophoretic parameter N_t. The growth in the thermophoretic parameter leads to higher thermophoretic force. Consequently, convective heat transfer decreases due to the increment of moving particles from the vicinity of the plate to its surroundings. Fig. 19 delineates the impact of magnetic parameter M and suction/injection parameters on the Skin friction coefficient. In Fig. 18, the Skin friction coefficient escalates by raising the values of the magnetic parameter for both suction and injection cases. This escalation in skin friction coefficient is the consequence of growth in Lorentz force due to an increase of magnetic parameter, which resists the velocity of the flow. So the wall friction increases, and therefore shear stress at the wall grows.

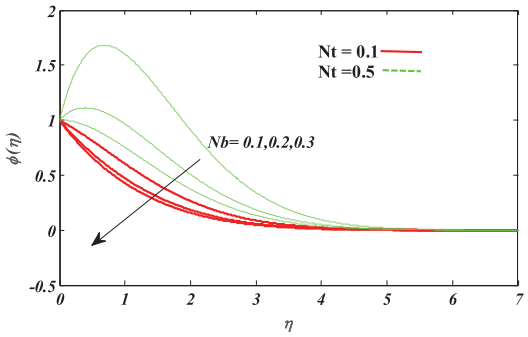

Figure 12: Effect of brownian motion parameter N_b on concentration profile using $Pr = 1.2,\ \epsilon = \ \delta = 0.1, R = 0.1,\ Sc = 01,\ M = \ \mathrm{f}_w = 0.5,\ \beta = -0.5$

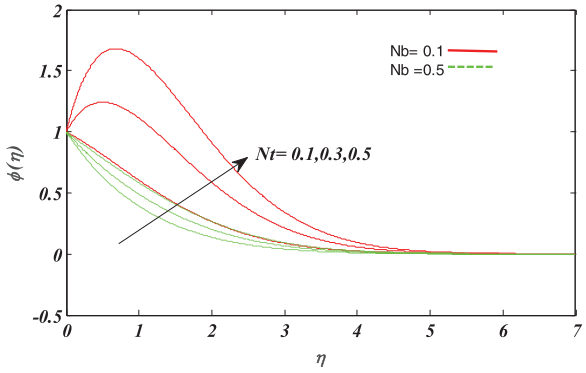

Figure 13: Effect of thermophoresis parameter N_t on concentration profile using $Pr = 1.2$, $\epsilon = 0.1$, $Sc = 01$, $R = 0.5$, $\delta = 0.1$, $\beta = 0.2$

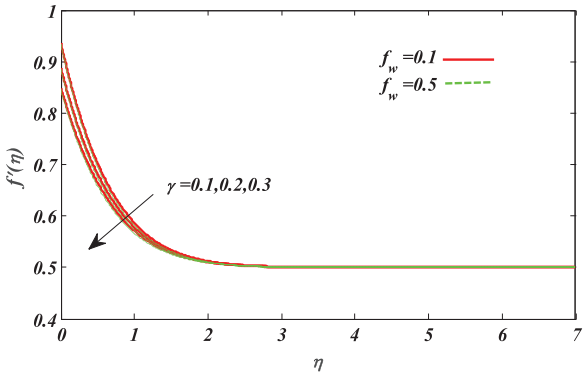

Figure 14: Effect of velocity slip parameter γ on the velocity profile using $Pr = 1.2$, $\epsilon = 0.1$, $Nb = Nt = 0.2$, $Sc = 01$, $R = M = 0.5$, $\delta = 0.1$

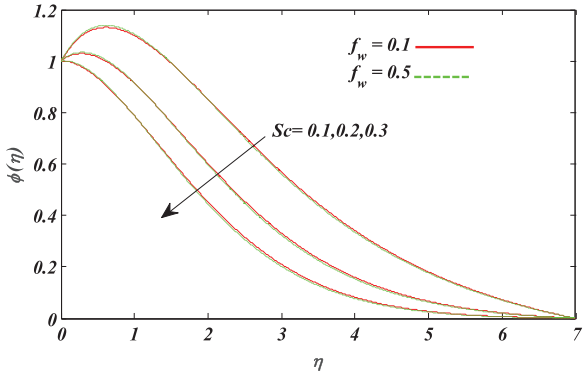

Figure 15: Effect of Schmidt number Sc on the concentration profile using $Pr = 1.2$, $\epsilon = 0.1$, $Nb = Nt = 0.2$, $Sc = 01$, $R = M = 0.5$, $\delta = 0.1$

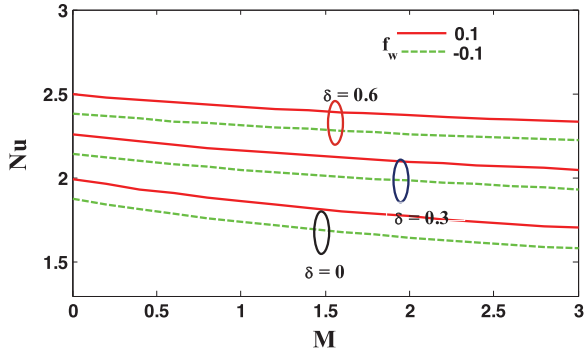

Figure 16: Effect of unsteady parameter δ & magnetic parameter M on local Nusselt number using $Pr = 1.2,\ \epsilon = 0.1,\ \ Nb = Nt = 0.2,\ R = Sc = 1,\ \beta = -0.5$

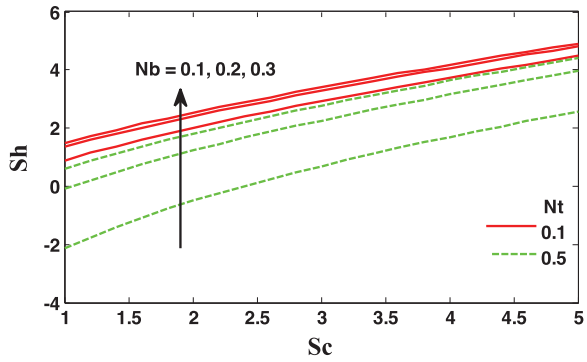

Figure 17: Effect of Schmidt number Sc & brownian motion parameter N_b on local Sherwood number using $Pr = 1.2,\ \epsilon = \delta = 0.1,\ M = \mathrm{f}_w = R = 0.5,\ \beta = -0.7$

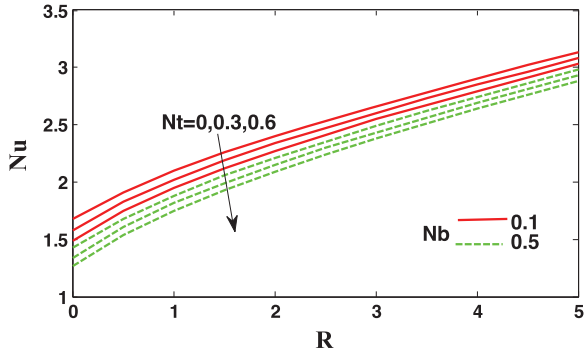

Figure 18: Effect of radiation parameter R & thermophoresis parameter N_t on local Nusselt number using $Pr = 1.2,\ \epsilon = \delta = 0.1,\ Sc = 01, M = \mathrm{f}_w = 0.5,\ \beta = 0.5,\ \gamma = 0.01$

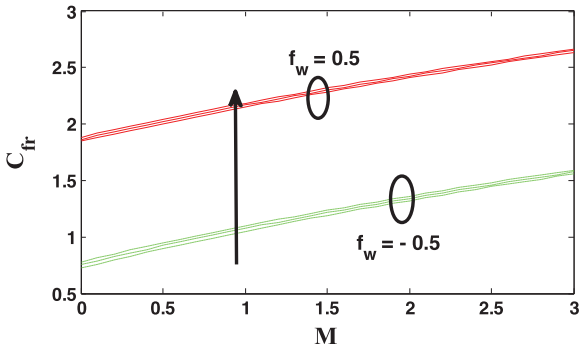

Figure 19: Effect of magnetic parameter M on skin friction coefficient using $\epsilon = 0.1,\ \beta = 0.5$

Figs. 20–22 show the surface plot and streamlines for velocity profile without using Maxwell fluid when the bottom wall's velocity moves in the right and left directions. The negative sign in the captions of these figures shows that the wall is moving in the negative x-axis direction. These figures are obtained using software that uses the finite element method to solve differential equations. One side in these figures shows an inlet, and two sides are outlets.

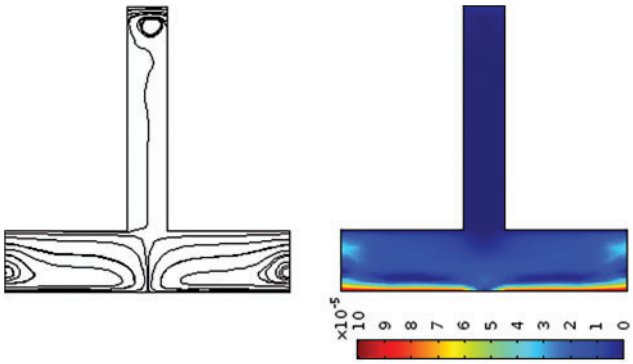

Figure 20: Surface plot and streamlines using $U_w = 0.0001$ & $U_w = -0.0001$

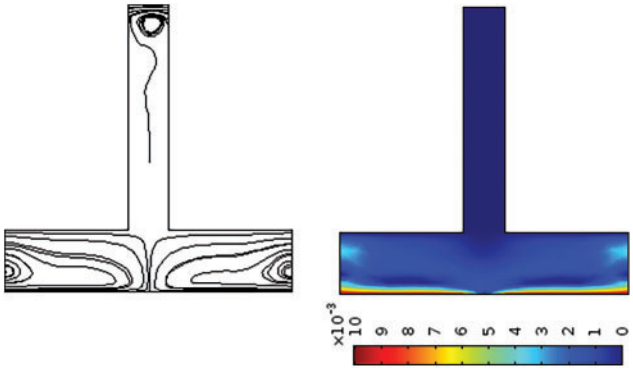

Figure 21: Surface plot and streamlines using $U_w = -0.01$ & $U_w = 0.01$

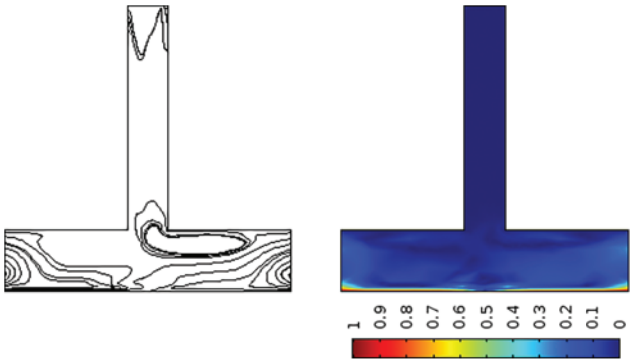

Figure 22: Surface plot and streamlines using $U_w = -1$ & $U_w = 1$

The comparison and validation of the current study with earlier studies for determining the numerical values of the skin friction coefficient are shown in Table 1. The current methodology employs the Runge-Kutta method in conjunction with an iterative method.

Table 1: Numerical values of $-f''(\eta)$ using $M = \gamma = \delta = f_w = 0$

ε	Mahparta et al. [52]	Nazar et al. [53]	Hayat el al. [54]	Mabood et al. [34]	Present
0.1	0.9694	0.9694	0.96938	0.96938	0.97069
0.2	0.9181	0.9181	0.91810	0.91811	0.91938
0.5	0.6673	0.6673	0.66732	0.66726	0.66828
1	-	0.0000	0.0000	0.0000	0.00000
2	−2.0175	−2.0175	−2.01750	−2.01750	−2.02250
3	−4.7293	−4.7296	−4.72928	−4.72928	−4.74429

The present investigation can be useful physically to generate some experimental estimates. When the impacts of various types of fluid on solid surfaces are investigated, the effects of various parameters can be valuable in avoiding time-consuming experiments. The primary benefit of conducting a theoretical investigation is that it saves time compared to conducting experiments.

Table 2 shows the approximate ranges of some physical parameters. For practical use, any value from these ranges can be chosen. The numerical values of parameters that can be used for any practical purpose can be chosen from this Table 2. Some ranges in Table 2 depends on the length of the domain. The solution can be obtained in some smaller domains.

Table 2: Approximate numerical ranges for some parameters using $N_t = 0.01$, $N_b = 0.01$, $M = 0.01$, $\delta = 0.0, 1$ and $\epsilon = 0.01$

Pr	Sc	β	γ	f_w	R
0.01 325 0.01	0.01 339	0.01	0.01	0.1	0.01

(Continued)

Table 2 (continued)

Pr	Sc	β	γ	f_w	R
	0.01				
	0.01	95			
		0.01	∞		
			0.01	9	
					∞

5 Conclusions

An existing mathematical model has been modified by considering Maxwell fluid and velocity slip boundary conditions. Moreover, the radiation and magnetic field in the unsteady flow are examined. Additionally, the effects of suction and insertion on fluid flow have been investigated. The concerning dimensional equations for the model, such as energy, momentum, and concentration equations, have been converted into non-dimensional ODEs by employing similarity transformations. In addition to this, outcomes of the variety of substantial parameters under observation on non-dimensional velocity, temperature, and concentration profiles have been delineated graphically. Summarizing all results and arguments, it is concluded that:

- The velocity profile decelerated with the escalation in M, whereas the temperature profile showed an opposite trend with suction/injection.
- Temperature, velocity, and concentration side views were seemed to decline for rising values of the unsteady parameter
- With the escalation in Maxwell, the parameter β velocity profile tended to decrease for both suction and injection.
- Temperature profiles escalated with the escalation in Thermophoresis, and the Brownian motion parameter, Whereas, Concentration profiles seemed to decelerate for the Brownian parameter. Still, profiles showed the opposite trend for the Thermophoretic parameter.
- Due to the magnetic parameter, M skin friction seemed to increase, whereas the heat transfer rate seemed to decrease monotonically; moreover, the heat transfer rate and skin friction inclined for the unsteady parameter δ.
- However, the heat transfer rate was escalated with an escalation in radiation parameter R. It reduced for rising values of the thermophoretic parameter.

With the escalation in Schmidt number S_c, mass transfer rate accelerated. Also, the mass transfer rate seemed to increase for the Brownian parameter N_b, whereas it decreased for the thermophoretic parameter N_t. Adding new effects to the model and studying the impact of various parameters on velocity, temperature, and concentration profiles analytically or numerically are possibilities in the future.

Acknowledgement: The authors wish to express their gratitude to Prince Sultan University for facilitating the publication of this article through the Theoretical and Applied Sciences Lab.

Funding Statement: The authors would like to acknowledge the support of Prince Sultan University for paying the Article Processing Charges (APC) of this publication.

Conflicts of Interest: The authors declare that they have no conflicts of interest to report regarding the present study.

References

1. Ahmed, A., Khan, M., Irfan, M., Ahmed, J. (2020). Transient MHD flow of maxwell nanofluid subject to non-linear thermal radiation and convective heat transport. *Applied Nanoscience, 10(12),* 5361–5373. DOI 10.1007/s13204-020-01375-1.
2. Bi, S., Li, Q., Yan, Y., Asare-Yeboah, K., Ma, T. et al. (2019). Layer-dependent anisotropic frictional behavior in two-dimensional monolayer hybrid perovskite/ITO layered heterojunctions. *Physical Chemistry Chemical Physics, 21(5),* 2540–2546. DOI 10.1039/C8CP06645K.
3. Bi, S., Li, Y., He, Z., Ouyang, Z., Guo, Q. et al. (2019). Self-assembly diketopyrrolopyrrole-based materials and polymer blend with enhanced crystal alignment and property for organic field-effect transistors. *Organic Electronics, 65,* 96–99. DOI 10.1016/j.orgel.2018.11.008.
4. Hayat, T., Aziz, A., Muhammad, T., Alsaedi, A., Mustafa, M. (2016). On magnetohydrodynamic flow of second grade nanofluid over a convectively heated non-linear stretching surface. *Advanced Powder Technology, 27(5),* 1992–2004. DOI 10.1016/j.apt.2016.07.002.
5. Hayat, T., Waqas, M., Shehzad, S. A., Alsaedi, A. (2016). Stretched flow of carreau nanofluid with convective boundary condition. *Pramana, 86(1),* 3–17. DOI 10.1007/s12043-015-1137-y.
6. Irfan, M., Khan, M., Khan, W. A. (2017). Numerical analysis of unsteady 3D flow of carreau nanofluid with variable thermal conductivity and heat source/sink. *Results in Physics, 7,* 3315–3324. DOI 10.1016/j.rinp.2017.08.029.
7. Ahmed, S. E., Mohamed, R. A., Aly, A. E. M., Soliman, M. S. (2019). Magnetohydrodynamic Maxwell nanofluids flow over a stretching surface through a porous medium: Effects of non-linear thermal radiation, convective boundary conditions and heat generation/absorption. *International Journal of Aerospace and Mechanical Engineering, 13(6),* 436–443.
8. Vittal, C., Vijayalaxmi, T., Reddy, C. K. (2018). MHD stagnation point flow and convective heat transfer of tangent hyperbolic nanofluid over a stretching sheet with zero normal flux of nanoparticles. *Journal of Nanofluids, 7(5),* 844–852. DOI 10.1166/jon.2018.1509.
9. Shravani, I., Ramya, D., Joga, S. (2018). Heat and mass transfer in stagnation point flow over a stretching sheet with chemical reaction and suction/injection in nanofluids. *Journal of Nanofluids, 7(5),* 862–869. DOI 10.1166/jon.2018.1511.
10. Srinivas, S., Malathy, T., Reddy, A. S. (2016). A note on thermal-diffusion and chemical reaction effects on MHD pulsating flow in a porous channel with slip and convective boundary conditions. *Journal of King Saud University-Engineering Sciences, 28(2),* 213–221. DOI 10.1016/j.jksues.2014.03.011.
11. Ramesh, G. K., Gireesha, B. J., Hayat, T., Alsaedi, A. (2016). Stagnation point flow of Maxwell fluid towards a permeable surface in the presence of nanoparticles. *Alexandria Engineering Journal, 55(2),* 857–865. DOI 10.1016/j.aej.2016.02.007.
12. Manjunatha, S., Gireesha, B. J. (2016). Effects of variable viscosity and thermal conductivity on MHD flow and heat transfer of a dusty fluid. *Ain Shams Engineering Journal, 7(1),* 505–515. DOI 10.1016/j.asej.2015.01.006.
13. Salahuddin, T., Malik, M. Y., Hussain, A., Awais, M., Khan, I. et al. (2017). Analysis of tangent hyperbolic nanofluid impinging on a stretching cylinder near the stagnation point. *Results in Physics, 7,* 426–434. DOI 10.1016/j.rinp.2016.12.033.
14. Ahmmed, S. F., Biswas, R., Afikuzzaman, M. (2018). Unsteady magnetohydrodynamic free convection flow of nanofluid through an exponentially accelerated inclined plate embedded in a porous medium with variable thermal conductivity in the presence of radiation. *Journal of Nanofluids, 7(5),* 891–901. DOI 10.1166/jon.2018.1520.

15. Hayat, T., Khan, M. I., Waqas, M., Alsaedi, A. (2017). Newtonian heating effect in nanofluid flow by a permeable cylinder. *Results in Physics, 7,* 256–262. DOI 10.1016/j.rinp.2016.11.047.
16. Mondal, S., Nandy, S. K., Sibanda, P. (2018). MHD flow and heat transfer of maxwell nanofluid over an unsteady permeable shrinking sheet with convective boundary conditions. *Journal of Nanofluids, 7(5),* 995–1003. DOI 10.1166/jon.2018.1506.
17. Choi, S. U., Eastman, J. A. (1995). Enhancing thermal conductivity of fluids with nanoparticles (No. ANL/MSD/CP-84938; CONF-951135-29). Argonne National Lab. (ANL), Argonne, IL USA.
18. Rashidi, M. M., Ganesh, N. V., Hakeem, A. A., Ganga, B. (2014). Buoyancy effect on MHD flow of nanofluid over a stretching sheet in the presence of thermal radiation. *Journal of Molecular Liquids, 198,* 234–238. DOI 10.1016/j.molliq.2014.06.037.
19. Sheikholeslami, M., Ellahi, R., Ashorynejad, H. R., Domairry, G., Hayat, T. (2014). Effects of heat transfer in flow of nanofluids over a permeable stretching wall in a porous medium. *Journal of Computational and Theoretical Nanoscience, 11(2),* 486–496. DOI 10.1166/jctn.2014.3384.
20. Mabood, F., Khan, W. A., Ismail, A. M. (2015). MHD boundary layer flow and heat transfer of nanofluids over a non-linear stretching sheet: A numerical study. *Journal of Magnetism and Magnetic Materials, 374,* 569–576. DOI 10.1016/j.jmmm.2014.09.013.
21. Sheikholeslami, M., Abelman, S., Ganji, D. D. (2014). Numerical simulation of MHD nanofluid flow and heat transfer considering viscous dissipation. *International Journal of Heat and Mass Transfer, 79,* 212–222. DOI 10.1016/j.ijheatmasstransfer.2014.08.004.
22. Ibrahim, W., Shankar, B. (2013). MHD boundary layer flow and heat transfer of a nanofluid past a permeable stretching sheet with velocity, thermal and solutal slip boundary conditions. *Computers & Fluids, 75,* 1–10. DOI 10.1016/j.compfluid.2013.01.014.
23. Hayat, T., Imtiaz, M., Alsaedi, A. (2016). Unsteady flow of nanofluid with double stratification and magnetohydrodynamics. *International Journal of Heat and Mass Transfer, 92,* 100–109. DOI 10.1016/j.ijheatmasstransfer.2015.08.013.
24. Mustafa, M., Khan, J. A., Hayat, T., Alsaedi, A. (2017). Buoyancy effects on the MHD nanofluid flow past a vertical surface with chemical reaction and activation energy. *International Journal of Heat and Mass Transfer, 108,* 1340–1346. DOI 10.1016/j.ijheatmasstransfer.2017.01.029.
25. Atif, S. M., Hussain, S., Sagheer, M. (2018). Numerical study of MHD micropolar carreau nanofluid in the presence of induced magnetic field. *AIP Advances, 8(3),* 035219. DOI 10.1063/1.5022681.
26. Dogonchi, A. S., Ganji, D. D. (2018). Effect of Cattaneo–Christov heat flux on buoyancy MHD nanofluid flow and heat transfer over a stretching sheet in the presence of Joule heating and thermal radiation impacts. *Indian Journal of Physics, 92(6),* 757–766. DOI 10.1007/s12648-017-1156-2.
27. Reddy, J. R., Sugunamma, V., Sandeep, N. (2018). Thermophoresis and brownian motion effects on unsteady MHD nanofluid flow over a slendering stretching surface with slip effects. *Alexandria Engineering Journal, 57(4),* 2465–2473. DOI 10.1016/j.aej.2017.02.014.
28. Dogonchi, A. S., Alizadeh, M., Ganji, D. D. (2017). Investigation of MHD go-water nanofluid flow and heat transfer in a porous channel in the presence of thermal radiation effect. *Advanced Powder Technology, 28(7),* 1815–1825. DOI 10.1016/j.apt.2017.04.022.
29. Hayat, T., Qayyum, S., Imtiaz, M., Alsaedi, A. (2016). Comparative study of silver and copper water nanofluids with mixed convection and non-linear thermal radiation. *International Journal of Heat and Mass Transfer, 102,* 723–732. DOI 10.1016/j.ijheatmasstransfer.2016.06.059.
30. Sheikholeslami, M. (2017). Magnetic field influence on nanofluid thermal radiation in a cavity with tilted elliptic inner cylinder. *Journal of Molecular Liquids, 229,* 137–147. DOI 10.1016/j.molliq.2016.12.024.
31. Sheikholeslami, M., Rashidi, M. M., Ganji, D. D. (2015). Effect of non-uniform magnetic field on forced convection heat transfer of Fe_3O_4–water nanofluid. *Computer Methods in Applied Mechanics and Engineering, 294,* 299–312. DOI 10.1016/j.cma.2015.06.010.

32. Serna, J. (2016). Heat and mass transfer mechanisms in nanofluids boundary layers. *International Journal of Heat and Mass Transfer, 92,* 173–183. DOI 10.1016/j.ijheatmasstransfer.2015.08.072.
33. Mastroberardino, A. (2014). Mixed convection in viscoelastic boundary layer flow and heat transfer over a stretching sheet. *Advances in Applied Mathematics and Mechanics, 6(3),* 359–375. DOI 10.4208/aamm.2013.m303.
34. Mabood, F., Khan, W. A. (2016). Analytical study for unsteady nanofluid MHD flow impinging on heated stretching sheet. *Journal of Molecular Liquids, 219,* 216–223. DOI 10.1016/j.molliq.2016.02.071.
35. Mahdy, A., Mansour, M. A., Ahmed, S. E., Mohamed, S. S. (2017). Entropy generation of Cu−water nanofluids through non-darcy porous medium over a cone with convective boundary condition and viscous dissipation effects. *Special Topics & Reviews in Porous Media: An International Journal, 8(1),* 59–72.
36. Rashad, A. M., Gorla, R. S. R., Mansour, M. A., Ahmed, S. E. (2017). Magnetohydrodynamic effect on natural convection in a cavity filled with a porous medium saturated with nanofluid. *Journal of Porous Media, 20(4),* 363–379.
37. Ahmed, S. E., Elshehabey, H. M. (2018). Buoyancy-driven flow of nanofluids in an inclined enclosure containing an adiabatic obstacle with heat generation/absorption: Effects of periodic thermal conditions. *International Journal of Heat and Mass Transfer, 124,* 58–73. DOI 10.1016/j.ijheatmasstransfer.2018.03.044.
38. Raizah, Z. A. S., Aly, A. M., Ahmed, S. E. (2018). Natural convection flow of a power-law non-newtonian nanofluid in inclined open shallow cavities filled with porous media. *International Journal of Mechanical Sciences, 140,* 376–393. DOI 10.1016/j.ijmecsci.2018.03.017.
39. Tlili, I., Naseer, S., Ramzan, M., Kadry, S., Nam, Y. (2020). Effects of chemical species and non-linear thermal radiation with 3D maxwell nanofluid flow with double stratification—An analytical solution. *Entropy, 22(4),* 453. DOI 10.3390/e22040453.
40. Khan, S. A., Nie, Y., Ali, B. (2020). Multiple slip effects on MHD unsteady viscoelastic nanofluid flow over a permeable stretching sheet with radiation using the finite element method. *SN Applied Sciences, 2(1),* 1–14.
41. Ahmad, I., Aziz, S., Ali, N., Khan, S. U., Khan, M. I. et al. (2020). Thermally developed Cattaneo-Christov maxwell nanofluid over bidirectional periodically accelerated surface with gyrotactic microorganisms and activation energy. *Alexandria Engineering Journal, 59(6),* 4865–4878. DOI 10.1016/j.aej.2020.08.051.
42. Ramzan, M., Shaheen, N., Chung, J. D., Kadry, S., Chu, Y. M. et al. (2021). Impact of newtonian heating and Fourier and fick's laws on a magnetohydrodynamic dusty casson nanofluid flow with variable heat source/sink over a stretching cylinder. *Scientific Reports, 11(1),* 1–19. DOI 10.1038/s41598-021-81747-x.
43. Mabood, F., Rauf, A., Prasannakumara, B. C., Izadi, M., Shehzad, S. A. (2021). Impacts of stefan blowing and mass convention on flow of Maxwell nanofluid of variable thermal conductivity about a rotating disk. *Chinese Journal of Physics, 71,* 260–272. DOI 10.1016/j.cjph.2021.03.003.
44. Bilal, S., Majeed, A. H., Mahmood, R., Khan, I., Seikh, A. H. et al. (2020). Heat and mass transfer in hydromagnetic second-grade fluid past a porous inclined cylinder under the effects of thermal dissipation, diffusion and radiative heat flux. *Energies, 13(1),* 278. DOI 10.3390/en13010278.
45. Lu, D., Afridi, M. I., Allauddin, U., Farooq, U., Qasim, M. (2020). Entropy generation in a dissipative nanofluid flow under the influence of magnetic dissipation and transpiration. *Energies, 13(20),* 5506. DOI 10.3390/en13205506.
46. Rafique, K., Anwar, M. I., Misiran, M., Khan, I., Seikh, A. H. et al. (2019). Brownian motion and thermophoretic diffusion effects on micropolar type nanofluid flow with soret and dufour impacts over an inclined sheet: Keller-box simulations. *Energies, 12(21),* 4191. DOI 10.3390/en12214191.
47. Khan, N. S., Gul, T., Kumam, P., Shah, Z., Islam, S. et al. (2019). Influence of inclined magnetic field on carreau nanoliquid thin film flow and heat transfer with graphene nanoparticles. *Energies, 12(8),* 1459. DOI 10.3390/en12081459.

48. Jamaludin, A., Nazar, R., Pop, I. (2019). Mixed convection stagnation-point flow of a nanofluid past a permeable stretching/shrinking sheet in the presence of thermal radiation and heat source/sink. *Energies, 12(5),* 788. DOI 10.3390/en12050788.
49. Bagherzadeh, S. A., Jalali, E., Sarafraz, M. M., Akbari, O. A., Karimipour, A. et al. (2019). Effects of magnetic field on micro cross jet injection of dispersed nanoparticles in a microchannel. *International Journal of Numerical Methods for Heat & Fluid Flow, 30(5),* 2683–2704. DOI 10.1108/HFF-02-2019-0150.
50. Jalali, E., Ali Akbari, O., Sarafraz, M. M., Abbas, T., Safaei, M. R. (2019). Heat transfer of oil/MWCNT nanofluid jet injection inside a rectangular microchannel. *Symmetry, 11(6),* 757. DOI 10.3390/sym11060757.
51. Hajatzadeh Pordanjani, A., Aghakhani, S., Karimipour, A., Afrand, M., Goodarzi, M. (2019). Investigation of free convection heat transfer and entropy generation of nanofluid flow inside a cavity affected by magnetic field and thermal radiation. *Journal of Thermal Analysis and Calorimetry, 137(3),* 997–1019. DOI 10.1007/s10973-018-7982-4.
52. Mahapatra, T., Gupta, A. S. (2002). Heat transfer in stagnation-point flow towards a stretching sheet. *Heat and Mass Transfer, 38(6),* 517–521. DOI 10.1007/s002310100215.
53. Nazar, R., Amin, N., Filip, D., Pop, I. (2004). Stagnation point flow of a micropolar fluid towards a stretching sheet. *International Journal of Non-Linear Mechanics, 39(7),* 1227–1235. DOI 10.1016/j.ijnonlinmec.2003.08.007.
54. Hayat, T., Javed, T., Abbas, Z. (2009). MHD flow of a micropolar fluid near a stagnation-point towards a non-linear stretching surface. *Nonlinear Analysis: Real World Applications, 10(3),* 1514–1526. DOI 10.1016/j.nonrwa.2008.01.019.
55. Kumbhakar, B., Sriniivasa Rao, P. (2015). Dissipative boundary layer flow over a nonlinearly stretching sheet in the presence of magnetic field and thermal radiation. *Proceedings of the National Academy of Sciences, India Section A: Physical Sciences, 85(1),* 117–125. DOI 10.1007/s40010-014-0187-8.
56. Nandi, S., Kumbhakar, B., Seth, G. S., Chamkha, A. J. (2021). Features of 3D magneto-convective non-linear radiative williamson nanofluid flow with activation energy, multiple slips and hall effect. *Physica Scripta, 96(6),* 065206. DOI 10.1088/1402-4896/abf009.
57. Seth, G. S., Sharma, R., Kumbhakar, B., Tripathi, R. (2017). MHD stagnation point flow over exponentially stretching sheet with exponentially moving free-stream, viscous dissipation, thermal radiation and non-uniform heat source/sink. In: *Diffusion foundations*, vol. 11, pp. 182–190. https://www.scientific.net/DF.11.182.
58. Mabood, F., Yusuf, T. A., Khan, W. A. (2021). Cu–Al_2O_3–H_2O hybrid nanofluid flow with melting heat transfer, irreversibility analysis and non-linear thermal radiation. *Journal of Thermal Analysis and Calorimetry, 143(2),* 973–984. DOI 10.1007/s10973-020-09720-w.
59. Yusuf, T. A., Mabood, F. (2020). Slip effects and entropy generation on inclined MHD flow of williamson fluid through a permeable wall with chemical reaction via DTM. *Mathematical Modelling of Engineering Problems, 7,* 1–9. DOI 10.18280/mmep.
60. Yusuf, T. A., Mabood, F., Gbadeyan, J. A., Adesanya, S. O. (2020). Non-linear convective flow of magnetohydrodynamic oldroyd 8-constant fluid in a channel with chemical reaction and convective boundary condition. *Journal of Thermal Science and Engineering Applications, 12(5),* 051022. DOI 10.1115/1.4046908.
61. Mabood, F., Yusuf, T. A., Bognár, G. (2020). Features of entropy optimization on MHD couple stress nanofluid slip flow with melting heat transfer and non-linear thermal radiation. *Scientific Reports, 10(1),* 1–13.
62. Mabood, F., Yusuf, T. A., Rashad, A. M., Khan, W. A., Nabwey, H. A. (2021). Effects of combined heat and mass transfer on entropy generation due to MHD nanofluid flow over a rotating frame. *Computers, Materials & Continua, 66(1),* 575–587. DOI 10.32604/cmc.2020.012505.

63. Arif, M. S., Nawaz, Y., Bibi, M., Ali, Z. (2018). Mass transfer of MHD nanofluid in presence of chemical reaction on a permeable rotating disk with convective boundaries, using buongiorno's model. *Computer Modeling in Engineering & Sciences, 116(1),* 31–49. DOI 10.31614/cmes.2018.00434.
64. Ejaz, A., Abbas, I., Nawaz, Y., Arif, M. S., Shatanawi, W. et al. (2020). Thermal analysis of MHD non-newtonian nanofluids over a porous media. *Computer Modeling in Engineering & Sciences, 125(3),* 1119–1134. DOI 10.32604/cmes.2020.012091.
65. Abdeljawad, T., Riaz, M. B., Saeed, S. T., Iftikhar, N. (2021). MHD Maxwell fluid with heat transfer analysis under ramp velocity and ramp temperature subject to non-integer differentiable operators. *Computer Modeling in Engineering & Sciences, 126(2),* 821–841. DOI 10.32604/cmes.2021.012529.
66. Aziz-Ur-Rehman, Riaz, M. B., Saeed, S. T., Yao, S. (2021). Dynamical analysis of radiation and heat transfer on MHD second grade fluid. *Computer Modeling in Engineering & Sciences, 129(2),* 689–703. DOI 10.32604/cmes.2021.014980.